PCCP

Physical Chemistry Chemical Physics

This paper was published in a themed issue of *PCCP* on:

Colloidal particles at liquid interfaces

Guest Editor: Professor B. P. Binks

Please take a look at the full table of contents for this issue

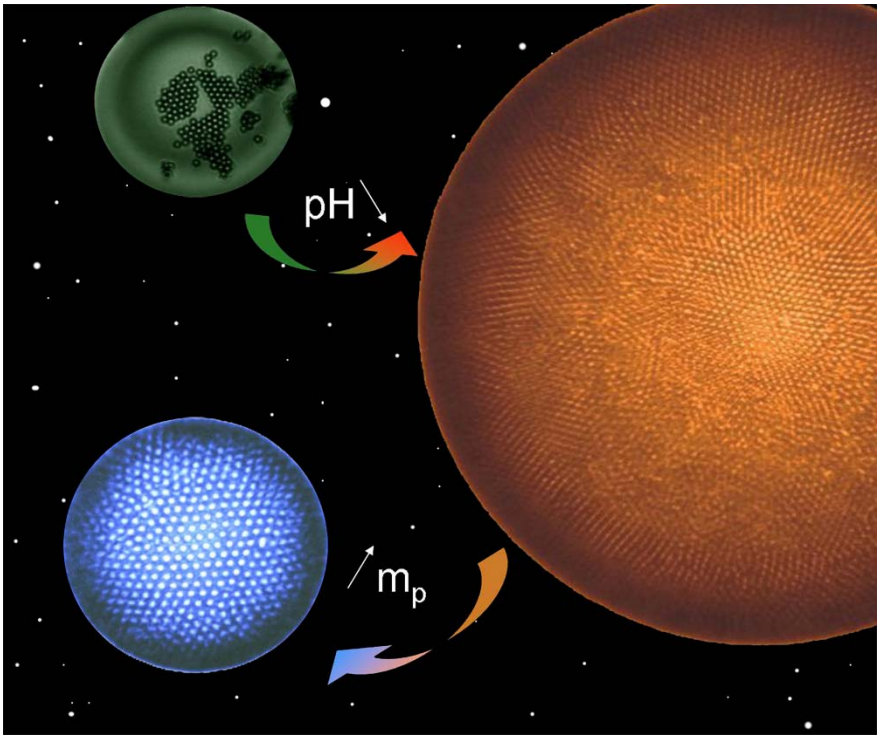

Papers in this issue include:

Stepwise interfacial self-assembly of nanoparticles *via* specific DNA pairing

Bo Wang, Miao Wang, Hao Zhang, Nelli S. Sobal, Weijun Tong, Changyou Gao, Yanguang Wang, Michael Giersig, Dayang Wang and Helmuth Möhwald, *Phys. Chem. Chem. Phys.*, 2007

DOI: 10.1039/b705094a

Water-in-carbon dioxide emulsions stabilized with hydrophobic silica particles

Stephanie S. Adkins, Dhiren Gohil, Jasper L. Dickson, Stephen E. Webber and Keith P. Johnston, *Phys. Chem. Chem. Phys.*, 2007

DOI: 10.1039/b711195a

Effect of electric-field-induced capillary attraction on the motion of particles at an oil–water interface

Mariana P. Boneva, Nikolay C. Christov, Krassimir D. Danov and Peter A. Kralchevsky, *Phys. Chem. Chem. Phys.*, 2007

DOI: 10.1039/b709123k

Effect of electric-field-induced capillary attraction on the motion of particles at an oil–water interface

Mariana P. Boneva, Nikolay C. Christov, Krassimir D. Danov and Peter A. Kralchevsky*

Received 15th June 2007, Accepted 6th September 2007
First published as an Advance Article on the web 14th September 2007
DOI: 10.1039/b709123k

Here, we investigate experimentally and theoretically the motion of spherical glass particles of radii 240–310 μm attached to a tetradecane–water interface. Pairs of particles, which are moving toward each other under the action of lateral capillary force, are observed by optical microscopy. The purpose is to check whether the particle electric charges influence the particle motion, and whether an electric-field-induced capillary attraction could be detected. The particles have been hydrophobized by using two different procedures, which allow one to prepare charged and uncharged particles. To quantify the hydrodynamic viscous effects, we developed a semiempirical quantitative approach, whose validity was verified by control experiments with uncharged particles. An appropriate trajectory function was defined, which should increase linearly with time if the particle motion is driven solely by the gravity-induced capillary force. The analysis of the experimental results evidences for the existence of an additional attraction between two like-charged particles at the oil–water interface. This attraction exceeds the direct electrostatic repulsion between the two particles and leads to a noticeable acceleration of their motion.

1. Introduction

The particle-stabilized (Pickering) emulsions and foams have attracted a considerable interest because of their potential applications for the development of novel materials and surfactant-free products.[1–4] The stability and properties of such emulsions are determined by the adsorption and structuring of particles on the surfaces of the emulsion drops. Dense and shell-like particle monolayers provide steric stabilization of the drops, prevent their flocculation and coalescence, and enhance the interfacial rheology.[1,2,5] In their own turn, the monolayer density, structure and rheology are influenced by the interparticle forces.

Interactions of electrostatic origin were found to significantly influence the type of particle structures at oil–water[6–10] and air–water[11] interfaces. Two-dimensional hexagonal arrays of particles were observed, in which the distance between the closest neighbors was markedly greater than the particle diameter.[6–11] The existence of such structures was explained by the action of electrostatic repulsion. In many cases, the particle arrays are insensitive to the concentration of electrolyte in the aqueous phase.[6,7,9] This fact, and the direct interparticle force measurements by laser tweezers,[7] lead to the conclusion that the electrostatic repulsion is due to charges at the particle–oil interface, which give rise to electric interactions across the oily phase.[6,7,9–11] Evidences for the presence of electric charges on the surface of solid particles dispersed in liquid hydrocarbons could be also found in earlier studies.[12,13]

Laboratory of Chemical Physics & Engineering, Faculty of Chemistry, University of Sofia, 1164 Sofia, Bulgaria. E-mail: pk@lcpe.uni-sofia.bg; Fax: +359 (0)2 962 5643; Tel: +359 (0)2 962 5310

In their experiments with 1.5 μm colloidal spheres at the surfaces of water droplets in oil, Nikolaides *et al.*[8] observed indications of attraction between like-charged particles, and attributed the observed effect to the action of electric-field-induced capillary attraction. Their work provoked a considerable interest, because the latter force could play an important role in the micrometer and submicrometer world,[14] where the effect of the gravity-induced lateral capillary force[15–20] is negligible.

Thus, particles attached to the interface between water and a nonpolar fluid (oil, air), could experience three forces of electric origin (Fig. 1): F_{ED}—electrodipping force;[21] F_{ER}—direct electric repulsion between the two particles across the nonpolar fluid,[6,7] and F_{EC}—electric-field-induced capillary attraction.[8] For brevity, the latter was also termed "electrocapillary attraction".[22] F_{ED} is normal to the oil–water

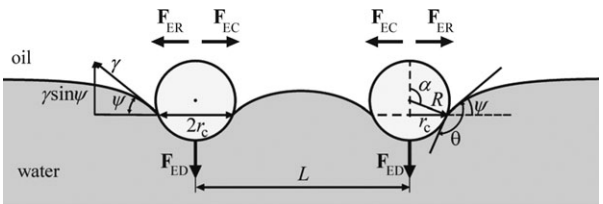

Fig. 1 Sketch of two electrically charged particles attached to an oil–water interface. F_{ED} is the electrodipping force, due to the image-charge effect, that pushes the particles into water and deforms the fluid interface around them. F_{ER} is the direct electric repulsion between the two like-charged particles. F_{EC} is the electrocapillary attraction, related to deformations in the fluid interface created by the electric field. R and r_c are the radii of the particle and contact line; θ and α are contact and central angles; ψ is the meniscus-slope angle at the contact line; γ is the oil–water interfacial tension.

interface and is directed toward the water (the phase with greater dielectric constant). Physically, F_{ED} is a result of the electrostatic image-charge effect.[23,24] F_{ED} is acting on each individual particle, while F_{ER} and F_{EC} are interaction forces between two (and more) particles. The electric field produces deformations (dimples) in the fluid interface around the particles.[25] In principle, the overlap of such deformations would lead to the appearance of F_{EC}.

At equilibrium, the electrodipping force is counterbalanced by the interfacial tension force: $F_{ED} = 2\pi r_c \gamma \sin\psi$, where r_c is the radius of the contact line on the particle surface; γ is the interfacial tension, and ψ is the meniscus-slope angle at the contact line (Fig. 1). Consequently, F_{ED} can be determined from the experimental values of r_c, γ, and ψ. This approach was used to determine F_{ED} for silanized glass particles of radii 200–300 μm at tetradecane–water and air–water interfaces.[21] F_{ED} was found to be much greater than the gravitational force acting on these particles. Numerical and analytical approaches to the calculation of F_{ED} and F_{ER} have been developed.[9,21,26]

As far as the theoretical description of F_{EC} is concerned, a generally accepted theory is still missing. The problem of the interplay of capillary and electric effects turned out to be rather complex. Controversial results have been reported based on the application of different truncated asymptotic expansions or other perturbation procedures.[27–30] Different approaches have lead to the conclusion that F_{EC} is attractive, but it is still unclear whether F_{EC} could prevail over F_{ER} under typical experimental conditions.[31–33] In the meantime, the amount of experimental evidence for the action of attractive forces between particles at fluid interfaces keeps increasing.[10,11,34–37]

In the present work, we undertake a direct experimental verification of the existence of electric-field-induced capillary attraction between two particles at an oil–water interface. Pairs of particles (of radius 240–310 μm), which are moving against each other under the action of a lateral capillary force, are observed by optical microscopy and the interparticle distance is recorded as a function of time. By analysis of the law of particle motion, one can obtain information regarding the acting forces. A similar approach has been applied to investigate immersion[38] and flotation[20] capillary forces. Here, our purpose is to check whether the particle electric charges influence the particle motion, and whether an electric-field-induced capillary attraction could be detected.

Section 2 describes the experimental systems and procedures. Section 3 gives the basis for a theoretical data interpretation, which takes into account the hydrodynamic interactions of the two moving particles. In Section 4, the results for pairs of charged and uncharged particles are compared and discussed.

2. Experimental

2.1 Materials and procedures

As already mentioned, in our experiments the nonpolar liquid phase was tetradecane ($C_{14}H_{30}$, for synthesis, Merck) of density $\rho_n = 0.763$ g cm^{-3} and viscosity $\eta_n = 2.3$ mPa s. The viscosity of the water phase is $\eta_w = 0.87$ mPa s. In some of our experiments, the water phase was an aqueous solution of 50 mM SDS (sodium dodecyl sulfate, Acros Organics USA), with added 50 mM NaCl (Merck). In other series of experiments, the aqueous phase was either pure water or a 0.1 mM solution of SDS without added NaCl. In Table 1, we have listed the values of the interfacial tension γ measured using the pendant drop method (apparatus DSA10-Mk2 Krüss, Hamburg), and of the characteristic capillary length, $q^{-1} = [\gamma/(\rho_w - \rho_n)g]^{1/2}$ for the respective two-phase liquid systems; $\rho_w \approx 1$ g cm^{-3} is the mass density of the water phase; g is the acceleration due to gravity.

Table 1 Interfacial tensions, γ, of the used aqueous phases against tetradecane, and the respective values of the capillary length, q^{-1}

Aqueous phase	γ/mN m^{-1}	q^{-1}/mm
50 mM SDS + 50 mM NaCl	5.45	1.54
0.1 mM SDS	43.8	4.35
Pure water	52.2	4.74

For the aqueous solution of 50 mM SDS + 50 mM NaCl, the surfactant concentration is *ca.* 20 times greater than the critical micelle concentration (CMC). For the solution of 0.1 mM SDS without NaCl, the surfactant concentration is *ca.* 80 times smaller than the CMC. All experiments were carried out at room temperature, 23 °C.

The used spherical particles were ballotini solid soda glass balls, supplied by Jencons-PLS (UK); mass density $\rho_p = 2.5$ g cm^{-3}. The radii of the used particles were in the range between 240 and 310 μm. We hydrophobized the particles by hexamethyldisilazane, $(CH_3)_3SiNHSi(CH_3)_3$ (HMDS, Sigma); the used procedures are described below.

After such a particle had been placed on the oil–water interface, we measured the meniscus-slope angle ψ (see Fig. 1) by side-view microscopic observations. The experimental value of ψ will be denoted by ψ_{exp}. In addition, from the mass densities of the oil, water and particle, and from the measured particle and contact-line radii, R and r_c, we calculated the gravitational force acting on the particle, F_g, in the same way as in ref. 21. (F_g is the difference between the particle weight and the buoyancy force.) Next, we calculated the gravitational value of ψ, which will be denoted by ψ_g. In view of Fig. 1, $\sin\psi_g = F_g/(2\pi r_c\gamma)$. If $\psi_{exp} = \psi_g$, the particles are not electrically charged. If $\psi_{exp} > \psi_g$, the particles are electrically charged. The difference between ψ_{exp} and ψ_g, is due to the electrodipping force; see ref. 21 for details.

Before the hydrophobization, the particles were subjected to the following cleaning procedure. First, they were immersed for 2 hours in sulfochromic acid at room temperature. Next, they were abundantly rinsed by water and immersed for 6 hours in a 0.01 M solution of NaOH at room temperature. Further, the particles were dried for 15 hours at 80 °C in a drier. At the next step, the particles were subjected to hydrophobization by using one of the following two alternative procedures:

In the first procedure, the particles were spread as a monolayer on the bottom of a small glass vessel where a small amount (10 drops) of HMDS was dropped by a micropipette. Thus, the particles had been initially immersed in a layer of HMDS. Next, the glass vessel was placed for 1 hour in a

vacuum drier at pressure −0.08 MPa, and at room temperature. During this period of time, the HMDS completely evaporates, but some amount of it adsorbs on the particle surfaces, which become hydrophobic in this way. Finally, the vessel with the particles was kept opened for 1 hour with free access to atmospheric air. The last step turned out to be important for the electrical charging of the particles. When this step (free access to air for 1 h) was applied, 70–80% of the particles were charged, whereas the remaining 20–30% were not charged. When we skipped this last step of the procedure, and we carried out the measurement of the angle ψ immediately after the particle hydrophobization, the fraction of the charged particles was only 10–40%.

In the second hydrophobization procedure, 5 ml of HMDS is poured at the bottom of a small cylindrical vessel, which is covered by a microporous glass filter. The particles are placed over this filter, and then the vessel is kept in the vacuum drier for 24 hours at pressure −0.09 MPa at room temperature. During this period of time, the HMDS evaporates; its vapors are passing only through the filter and a part of them adsorbs on the glass particles. The glass particles prepared in this way are hydrophobic (with contact angle θ = 123–148°). However, the measurements of the meniscus-slope angle, ψ, with these particles shows that they are not electrically charged ($\psi_{exp} \approx \psi_g$). We used such particles in control experiments, in which we checked how correctly we were calculating the hydrodynamic force acting on particles that are moving on the oil–water interface (see Section 4.1).

We should also mention that (just as in ref. 21) the addition of NaCl to the aqueous phase does not influence the magnitude of ψ_{exp} in the case of charged particles. This indicates that the electrodipping force acting on the particle is due to electric charges located on the particle–oil (rather than on the particle–water) interface; see ref. 21 for details.

The particle radius R, the contact line radius r_c, the contact angle θ, and the meniscus-slope angle ψ (Fig. 1), vary from particle to particle. However, for each separate particle these geometrical parameters can be accurately measured from side-view photographs. Detailed data for the particles used in our experiments are presented in Section 4. The main goal of our experiments is to check whether there is a difference between the motion of pairs of charged and uncharged particles that are attached to the oil–water interface. This would reveal whether any effect of electric-field-induced capillary attraction could be detected. The problem concerning the origin of the electric charges at the particle–oil interface, which deserves a special attention, is out of the scope of the present study. The finding that the exposition of the hydrophobized particles to contact with the atmospheric air is important for their charging could have different explanations. For example, it is possible that the products of the reaction of HMDS with the glass surface subsequently interact with O_2 and/or H_2O molecules present in the air. It is also possible that some ions present in the atmosphere adsorb on the particle surfaces under the action of the attractive electrostatic image-charge force or due to specific interaction with the hydrophobizing coating. The clarification of the origin of the surface electric charges could be a subject of a separate study.

2.2 Experiments with pairs of particles

These experiments were carried out in a rectangular glass cell. The length, width and height of the cell were 80, 25 and 55 mm, respectively. The motion of the particles was observed using a horizontal optical system and recorded by a CCD camera (SONY XT-ST50CE) connected to a video-cassette recorder. The movies were digitized by a video capture board.

The experiments are performed in the following way. The aqueous and oily phases are consecutively poured in the cell, and are equilibrated for about 30 min. A pair of hydrophobized particles of approximately equal diameters is selected. One of the particles is placed on the interface and the geometrical parameters R, r_c, θ and ψ (Fig. 1) are measured at a high magnification from the respective photograph. After that, the magnification is reduced, and the second particle is gently dropped near the first one on the horizontal oil–water interface. If the distance between the particles is not too long, they begin to move toward each other. A typical video-frame is shown in Fig. 2a. Consecutive positions of two moving particles are shown by circles in Fig. 2b.

When the particles come into contact, the magnification is increased again (Fig. 3) to determine precisely the geometrical parameters of the second particle. In this case, the angles θ and ψ are measured at the outer side of the particle; ψ is measured with respect to the plane of the contact line, which might slightly differ from the horizontal plane. We checked that the values of the angles θ and ψ determined in this way are the same as those determined for a single particle in isolation.

From the record of the particle motion, we selected a series of video frames corresponding to a given sequence of time moments. On every selected video frame, we fitted a circle on the periphery of each particle (Fig. 2b), and the coordinates x_1 and x_2 of the centers of the two particles were determined. In this way, their trajectories, $x_1(t)$ and $x_2(t)$, were obtained. Here, t is time; the x-axis is oriented along the long side of the vessel (of length 80 mm). Along the y-axis (the short side of the vessel, 25 mm), the cross-section of the oil–water interface corresponds to a slightly concave meniscus. Although its

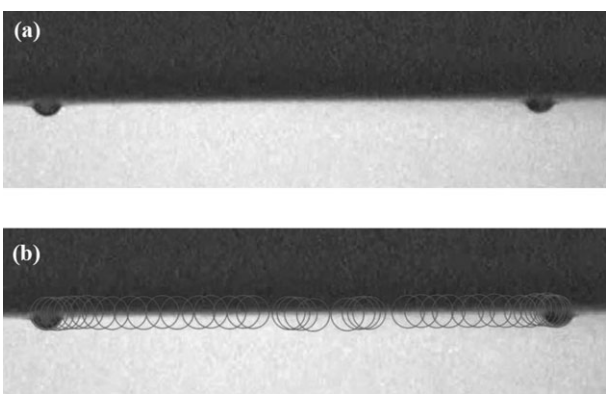

Fig. 2 (a) Side-view photograph of two interacting hydrophobized glass particles of radii R_1 = 281 μm, R_2 = 301 μm (pair 4) at the interface between tetradecane and water solution of 50 mM SDS + 50 mM NaCl. (b) Consecutive positions of the same two particles, which are moving toward each other, are shown by circles.

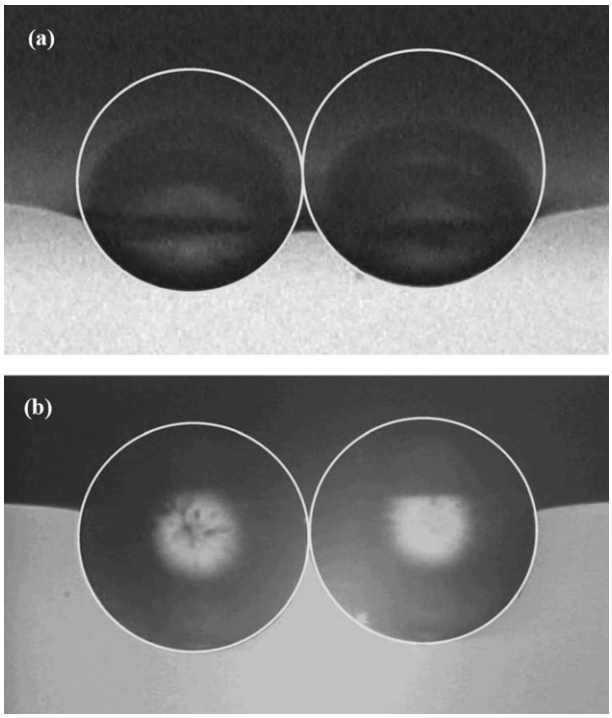

Fig. 3 Photographs of hydrophobized glass particles at close contact. (a) Particles of radii $R_1 = 281$ μm, $R_2 = 301$ μm (pair 4) at the interface between tetradecane and water solution of 50 mM SDS + 50 mM NaCl; $\gamma = 5.45$ mN m^{-1}. (b) Particles of radii $R_1 = 275$ μm, $R_2 = 269$ μm (pair 12) at the interface between tetradecane and water solution of 0.1 mM SDS; $\gamma = 43.8$ mN m^{-1}.

curvature is very small, it is sufficient to ensure particle motion along the x-axis, in the central part of the cell, parallel to its longer walls.

We carried out experiments with many pairs of particles. In Section 4, we report data for twelve pairs, which are representative for the following three series of experiments:

First, we used pairs of uncharged hydrophobic particles, produced by means of the second hydrophobization procedure (Section 2.1), which are attached to the boundary between tetradecane and a solution of 50 mM SDS + 50 mM NaCl. This relatively high concentration of SDS (≈20 times the CMC) was chosen because we expected that the fast supply of SDS monomers from the surfactant micelles would suppress the surface elasticity gradients (the Marangoni–Gibbs effect); otherwise, the latter could give rise to an additional hydrodynamic resistance to the particle motion.[39] The data for pairs No. 1, 2, 3 and 4 are representative for the experiments carried out under these conditions. As an illustration, Fig. 4 shows the trajectories $x_1(t)$ and $x_2(t)$ for pairs No. 1 and 4. The trajectories of all other pairs of particles look very similar to those shown in Fig. 4.

Second, we used pairs of charged particles, produced by means of the first hydrophobization procedure (Section 2.1), which are attached to the boundary between tetradecane and pure water. In this case, effects of surface rheology on the particle motion are not expected. The data for pairs No. 5, 6, 7 and 8 are representative for the experiments carried out under these conditions.

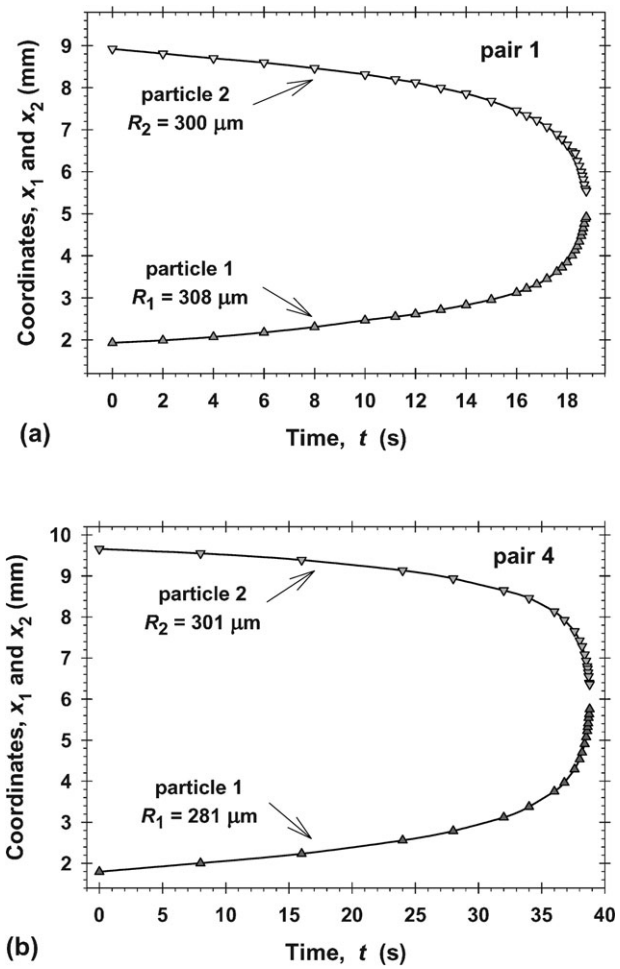

Fig. 4 Experimental trajectories, $x_1(t)$ and $x_2(t)$, of two particles moving toward each other: (a) pair 1; (b) pair 4. The particle radii are shown in the figure.

Third, we used pairs of charged particles, produced by means of the first hydrophobization procedure (Section 2.1), which were attached to the boundary between tetradecane and a solution of 0.1 mM SDS without added NaCl. At this relatively low concentration, the surfactant adsorption monolayer is diluted and, consequently, pronounced surface rheological effects are not expected. We wanted to check whether the presence of ionic surfactant at the interface would produce some effect on the motion of the charged particles. The data for pairs No. 9, 10, 11 and 12 are representative for the experiments carried out under these conditions (see Section 4 for details on the results).

3. Theoretical section

3.1 The law of particle motion

Here, we consider two submillimeter spheres, particle 1 and particle 2, which are attached to the interface between two fluids. In general, the particles are different. Their geometrical parameters are denoted by subscripts "1" and "2": particle radii R_1 and R_2; contact-line radii $r_{c,1}$ and $r_{c,2}$; contact angles θ_1 and θ_2; meniscus-slope angles ψ_1 and ψ_2. We assume that

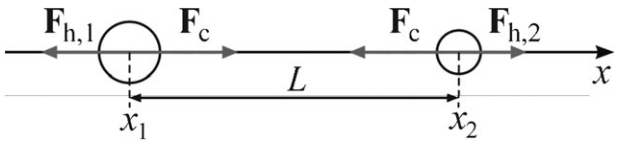

Fig. 5 Sketch of the forces acting on two particles attached to a liquid interface: $\mathbf{F}_c$ is the force of capillary attraction; $\mathbf{F}_{h,1}$ and $\mathbf{F}_{h,2}$ are the hydrodynamic drag forces.

the particles are moving toward each other driven by an attractive capillary force, F_c. In general, F_c could include contributions of gravitational and electric origin, $F_{c,g}$ and $F_{c,el}$:[21]

$$F_c = F_{c,g} + F_{c,el} \tag{1}$$

By definition, $F_{c,g}$ is the lateral capillary force in the absence of any electric effects.[15–20] Newton's second law, applied to the considered particles, reads:

$$m_1 \frac{d^2 x_1}{d\,t^2} = F_c - F_{h,1}, \quad m_2 \frac{d^2 x_2}{d\,t^2} = -F_c + F_{h,2} \tag{2}$$

Here, m_1 and m_2 are the masses of the two particles; as before, x_1 and x_2 are the x-coordinates of their centers; the particles are moving along the x-axis. $F_{h,1}$ and $F_{h,2}$ are the hydrodynamic resistance (friction) forces acting on the two particles; each of them is directed opposite to the direction of motion of the respective particle (Fig. 5).

First, let us estimate the relative importance of the inertia term in eqn (2).

$$m_1 \frac{d^2 x_1}{dt^2} / F_{h,1} \approx (m_1 \frac{d^2 x_1}{dt^2}) / (6\pi\eta R_1 \frac{dx_1}{dt}) = \frac{2\rho_p R_1^2}{9\eta t_{exp}} = 0.02 \tag{3}$$

where the following typical parameter values have been substituted: particle mass density $\rho_p = 2.6$ g cm^{-3}; particle radius $R_1 = 250$ μm; viscosity $\eta = 1.5\times10^{-3}$ Pa s; characteristic experimental period of time $t_{exp} = 1$ s. At smaller distances between the particles, the hydrodynamic resistance increases (because of the interparticle hydrodynamic interaction) and, consequently, the ratio in eqn (3) becomes even smaller. For the conditions of our experiments, the Reynolds number is also small because of the small particle radii and low velocities of motion. Neglecting the acceleration terms in eqn (2), and using the fact that at small Reynolds numbers the hydrodynamic resistance force is proportional to the particle velocity, $F_{h,k} = \beta_k(dx_k/dt)$, $k = 1, 2$, we bring eqn (2) into the form:

$$\beta_1 \frac{dx_1}{dt} = F_c \quad \text{and} \quad \beta_2 \frac{dx_2}{dt} = -F_c \tag{4}$$

where β_1 and β_2 are the hydrodynamic resistances for the particles 1 and 2, respectively. The center-to-center interparticle distance is:

$$L = x_2 - x_1 \tag{5}$$

The subtraction of the two expressions in eqn (4) yields:

$$\frac{dL}{dt} = -\left(\frac{1}{\beta_2} + \frac{1}{\beta_1}\right) F_c \tag{6}$$

Eqn (6) is basic for the procedure of data processing described in Section 3.4.

3.2 Expression for the hydrodynamic drag force

Here, our task is to estimate the hydrodynamic resistances β_1 and β_2. The problem of the two-dimensional motion of particles attached to the interface between two viscous fluid phases has been exactly solved only in the case of a single particle at a planar interface in the absence of surface elasticity (due to adsorbed surfactant).[40–43] This includes the case when the interface exhibits a purely viscous behavior that could be realized at surfactant concentrations above the CMC, for which the fast exchange of surfactant molecules between the interface and the micelles suppresses the surface elasticity.[39] So far, exact solutions of the hydrodynamic problem are missing in the cases when the following effects are significant:

(a) In the presence of *surface elasticity* (the Marangoni effect) due to adsorbed surfactant. For soluble surfactants, this problem includes compression and desorption of surfactant molecules in front of the moving particle, accompanied by monolayer expansion and adsorption from the bulk behind the moving particle.

(b) In the presence of a *dimple* (concave meniscus) created by the particle in the fluid interface (as sketched in Fig. 1), the experimental friction coefficient is markedly greater[41] than the one theoretically calculated for a planar fluid interface without dimple. However, a theoretical expression for estimating the increased hydrodynamic resistance due to the dimple is still missing.

(c) In the presence of *hydrodynamic interaction* between two particles that are moving against each other attached to the interface between two viscous fluid phases.

For our experimental situation, the effect (a) is expected to be negligible, but the effects (b) and (c) are significant. The effect (b) leads only to a greater hydrodynamic resistance (a greater multiplicative constant β_k), whereas the effect (c) is especially important because it depends on the distance between the two particles, L, and interferes with the dependence $F_c(L)$. For this reason, our first goal is to obtain an approximate expression describing the effect (c).

In the case of small Reynolds numbers, the problem of the hydrodynamic interaction between two identical spherical particles of radius R moving against each-other with velocity U in a fluid of viscosity η has been solved by Stimson and Jeffery.[44] Their exact result for the hydrodynamic force, F_h, acting on each particle reads:

$$F_h = \beta U, \quad \beta \equiv 6\pi\eta R f_h(s, R) \tag{7}$$

where β is the hydrodynamic resistance and $f_h(s, R)$ is the drag coefficient; $s = L - 2R$ is the shortest surface-to-surface distance between the two particles: the dependence $f_h(s, R)$ has been obtained in the form of series:[44]

$$f_h(s,R) = \frac{\sinh w}{3} \sum_{n=1}^{\infty} \frac{n(n+1)}{\Delta_n} \left\{ \frac{2n+1}{2(2n-1)} \exp(2w) + \frac{2n+1}{2(2n+3)} \exp(-2w) + \frac{4\exp[-(2n+1)w]}{(2n-1)(2n+3)} - 1 \right\} \tag{8}$$

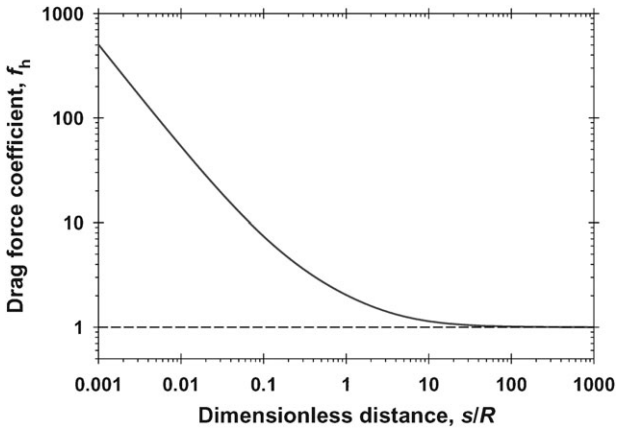

Fig. 6 Plot of the drag force coefficient, f_h, *vs.* s/R, calculated using eqn (8). At long interparticle distances, we have $f_h \to 1$, which corresponds to Stokes friction. At shorter distances, we have $f_h > 1$ due to the hydrodynamic interaction between the two spherical particles.

where

$$\cosh w \equiv 1 + \frac{s}{2R} \text{ and}$$

$$\Delta_n \equiv \sinh[(2n+1)w] - \frac{2n+1}{2}\sinh(2w) \qquad (9)$$

$$(n = 1,\ 2,...)$$

For large interparticle distances, $s \to \infty$, eqn (8) yields $f_h \to 1$ (see Fig. 6), and then eqn (7) reduces to the Stokes formula, $\beta = 6\pi\eta R$. In the opposite limit, when $s/R << 1$ and the particles are close to each other, eqn (8) gives asymptotically the Taylor formula:[45]

$$f_h(s, R) \approx \frac{R}{2s} \text{ and } F_h \approx \frac{3\pi\eta R^2}{s} U \qquad (10)$$

The plot of f_h *vs.* s/R, calculated from eqn (8) and (9) is shown in Fig. 6. One sees that f_h increases by orders of magnitude when s decreases. For this reason, the accounting for the hydrodynamic interaction is essential when interpreting our experimental data.

The series in eqn (8) can be summed up numerically with a high precision. For faster computations, one could use the interpolation formula

$$f_h(s, R) \approx \left(1 + \frac{R}{2s}\right)\left\{1 + 0.3766\exp\left[-\frac{(\ln s - \ln R + 0.6789)^2}{6.297}\right]\right\} \qquad (11)$$

The relative error of eqn (11) is smaller than 0.015 for all values of the ratio s/R.

If the two particles have different radii, R_1 and R_2, then instead of eqn (10) we have:[46]

$$f_h(s, R_m) = \frac{R_m}{2s} \qquad (12)$$

where $s = L - R_1 - R_2$, and R_m is a mean particle radius defined as follows:[46]

$$\frac{1}{R_m} \equiv \frac{1}{2}\left(\frac{1}{R_1} + \frac{1}{R_2}\right) \qquad (13)$$

Furthermore, with the help of the definition

$$\beta_k = 6\pi\eta R_k f_h(s, R_m),\ k = 1,\ 2 \qquad (14)$$

we obtain:

$$\frac{1}{\beta_1} + \frac{1}{\beta_2} = \frac{1}{6\pi f_h(s, R_m)}\left(\frac{1}{\eta R_1} + \frac{1}{\eta R_2}\right) \qquad (15)$$

In eqn (15) one can use eqn (8) to calculate $f_h(s, R_m)$. Thus, at $s \to \infty$ we have $f_h \to 1$ and eqn (15) gives the result of the Stokes formula, whereas at $s \to 0$ it gives the result of the Taylor formula.

Finally, for the motion of two particles which are attached to the boundary between water and a nonpolar fluid, we will use the following semiempirical generalization of eqn (15):

$$\frac{1}{\beta_1} + \frac{1}{\beta_2} = \frac{1}{6\pi f_h(s, R_m)}\left(\frac{1}{\eta_1 R_1} + \frac{1}{\eta_2 R_2}\right) \qquad (16)$$

where η_1 and η_2 are the mean by area values of the viscosities of the two fluid phases:

$$\eta_1 \equiv \frac{\eta_n A_{n,1} + \eta_w A_{w,1}}{A_{n,1} + A_{w,1}}\ ;\eta_2 \equiv \frac{\eta_n A_{n,2} + \eta_w A_{w,2}}{A_{n,2} + A_{w,2}} \qquad (17)$$

Here, the subscripts "n" and "w" denote quantities related to the nonpolar fluid and water, respectively. In particular, η_n and η_w are the viscosities of the respective phases; $A_{n,1}$ and $A_{n,2}$ are the contact areas of particles 1 and 2 with the nonpolar fluid; $A_{w,1}$ and $A_{w,2}$ are the contact areas of particles 1 and 2 with the water phase:

$$A_{n,k} = 2\pi R_k[R_k \pm (R_k^2 - r_{c,k}^2)^{1/2}] \text{ and}$$
$$A_{w,k} = 4\pi R_k^2 - A_{n,k} \qquad (18)$$

In eqn (18), the sign is '+' when the central angle α (Fig. 1) is obtuse, and '−' when α is acute. The quantities in the denominators in eqn (17) represent the total surface areas of the respective particles. In eqn (16) and (17), we have taken into account the fact that the friction of a particle with each of the two adjacent fluid phases is expected to depend on the relative contact area of the particle with the respective fluid phase.

3.3 Gravity-induced capillary force

Here, we consider a pair of small uncharged particles for which $\sin^2\psi_{g,k} \ll 1$ and $(qr_{c,k})^2 \ll 1$ ($k = 1, 2$). In this case, the gravity-induced capillary force is described by the expression:[15–19]

$$F_{c,g} \approx 2\pi\gamma Q_1 Q_2 q K_1(qL) \qquad (19)$$

where K_1 is the modified Bessel function of the second kind and first order; $Q_k = r_{c,k}\sin\psi_{g,k}$ ($k = 1, 2$) is the so called "capillary charge" of the respective particle. On the other hand, the vertical balance of the forces acting on each particle yields:

$$F_{g,k} = 2\pi\gamma r_{c,k}\sin\psi_{g,k} = 2\pi\gamma Q_k\ (k = 1, 2) \qquad (20)$$

where $F_{g,k}$ is the gravitational force (particle weight minus buoyancy force) acting on the respective particle. Substituting

Q_1 and Q_2 from eqn (20) into eqn (19), we obtain:

$$F_{c,g} \approx \frac{F_{g,1}F_{g,2}}{2\pi\gamma} qK_1(qL) \quad (21)$$

The gravitational forces $F_{g,1}$ and $F_{g,2}$ can be presented in the form:[47,48]

$$F_{g,k} = F_{p,k} - F_{m,k} \; (k = 1, 2) \quad (22)$$

$F_{p,k}$, is a contribution from the particle itself:

$$F_{p,k} = (\rho_p - \rho_w)gV_{w,k} + (\rho_p - \rho_n)gV_{n,k} \; (k = 1, 2), \quad (23)$$

while $F_{m,k}$, is a contribution from the meniscus (dimple) formed around the particle:

$$F_{m,k} = (\rho_w - \rho_n)g\pi r_{c,k}^2 h_{g,k} \; (k = 1, 2) \quad (24)$$

$V_{w,k}$ and $V_{n,k}$ are the portions of the particle volume which are immersed, respectively, in the water phase and in the nonpolar fluid; $h_{g,k}$ is the depth of the meniscus (in the absence of any electric effects), *i.e.* the distance from the plane of the contact line to the plane of the horizontal interface far from the particles. By geometrical considerations, we obtain:

$$V_{n,k} = \frac{2}{3}\pi R_k^2[R_k \pm (R_k^2 - r_{c,k}^2)^{1/2}] \pm \frac{\pi}{3} r_{c,k}^2 (R_k^2 - r_k^2)^{1/2} \quad (25)$$

$$V_{w,k} = \frac{4}{3}\pi R_k^3 - V_{n,k} \quad (26)$$

In eqn (26), the sign is '+' when the central angle α (Fig. 1) is obtuse, and '–' when α is acute. In addition, $h_{g,k}$ can be estimated from the expression:[15–19]

$$h_{g,k} \approx \frac{F_{p,k}}{2\pi\gamma} K_0(qr_{c,k}) \quad (27)$$

where K_0 is the modified Bessel function of the second kind and zero order, and $F_{p,k}$ is given by eqn (23).

Finally, the gravitational value of the meniscus-slope angle (in the absence of any electric effects) is determined from eqn (20):

$$\sin\psi_{g,k} \equiv F_{g,k}/(2\pi\gamma r_{c,k}) \; (k = 1, 2) \quad (28)$$

where γ and $r_{c,k}$ are experimentally measured, whereas $F_{g,k}$ is calculated using eqn (22)–(27).

3.4 Procedure for data processing

Here, our aim is to describe quantitatively the time dependence of the interparticle distance, $L(t)$, assuming that the two particles are moving toward each other under the action of the gravity-induced lateral capillary force, $F_{c,g}$, *i.e.* assuming that electric effects are missing. For this goal, we substitute eqn (16) and (21) (the latter with $F_c = F_{c,g}$) into eqn (6):

$$\frac{dL}{dt} = -\frac{qF_{g,1}F_{g,2}}{12\pi^2\gamma}\left(\frac{1}{\eta_1 R_1} + \frac{1}{\eta_2 R_2}\right)\frac{K_1(qL)}{f_h(s, R_m)} \quad (29)$$

Having in mind that $s = L - R_1 - R_2$, in the left-hand side of eqn (29) we group the terms that depend on L. Next, by integration we obtain:

$$\Theta(L) = \tau(t - t_0) \quad (30)$$

where the "trajectory function" $\Theta(L)$ is defined as follows:

$$\Theta(L) \equiv \int_L^{L_0} q\frac{f_h(\tilde{s}, R_m)}{K_1(q\tilde{L})} d\tilde{L} \quad (31)$$

Here, $\tilde{L}$ is an integration variable; $\tilde{s} \equiv \tilde{L} - R_1 - R_2$; t_0 is the initial moment; $L_0 = L(t_0)$ is the interparticle distance at that moment. The coefficient τ in eqn (30) is defined by the expression:

$$\tau \equiv \frac{q^2 F_{g,1}F_{g,2}}{\pi\gamma\beta_m} \quad (32)$$

where β_m is a mean hydrodynamic resistance defined as follows:

$$\frac{1}{\beta_m} \equiv \frac{1}{2}\left(\frac{1}{6\pi\eta_1 R_1} + \frac{1}{6\pi\eta_2 R_2}\right) \quad (33)$$

The procedure of data processing is the following:

1. The input parameters are R_1; R_2; $r_{c,1}$; $r_{c,2}$; ρ_p; ρ_w; ρ_n; g; γ and $q = [(\rho_w - \rho_n)g/\gamma]^{1/2}$, as well as the experimental dependence $L(t)$.

2. From eqn (22)–(28) we calculate $V_{w,k}$; $V_{n,k}$; $F_{p,k}$; $h_{g,k}$; $F_{m,k}$; $F_{g,k}$ and $\psi_{g,k}$ for $k = 1, 2$.

3. From eqn (17) and (18) we calculate $A_{w,k}$; $A_{n,k}$ and η_k for $k = 1, 2$.

4. From eqn (32) and (33) we calculate β_m and τ.

5. For each pair of experimental values (t, L) we calculate $\Theta(L)$ by numerical integration of eqn (31), where $f_h(s, R_m)$ is determined by eqn (8) or (11), and R_m is given by eqn (13). Next, we plot $\Theta(L)$ *vs.* t. This dependence will be denoted by $\Theta_{exp}(t)$.

6. The theoretical linear dependence Θ *vs.* t is calculated from eqn (30) with τ determined at step 4 above. This linear dependence will be denoted by $\Theta_{theor}(t)$.

7. Finally, $\Theta_{exp}(t)$ and $\Theta_{theor}(t)$ are compared.

4. Results and discussion

4.1 Results for pairs of uncharged particles

Table 2 shows data for the particle pairs No. 1, 2, 3 and 4, which serve as "passports" identifying the respective particles. The values of R_k, $r_{c,k}$, θ_k and $\psi_{exp,k}$ are experimental (measured from the side-view video frames), whereas the values of the remaining parameters in this table are calculated as explained in Section 3.4. The values of the contact angle, θ_k, varying between 122 and 148° indicate that the investigated particles are pronouncedly hydrophobic.

The comparison of the last two rows of Table 2 shows that the *calculated* gravitational meniscus-slope angle, $\psi_{g,k}$, coincides with the *experimental* meniscus-slope angle, $\psi_{exp,k}$, in the framework of the accuracy of the goniometric measurement of $\psi_{exp,k}$. Hence, indications on the action of electrodipping force are missing for the considered particles. In other words, these particles are uncharged (the number of electric charges at the particle–oil interface is negligible).

Fig. 7 shows the experimental time-dependences, $L = L(t)$, of the center-to-center distance between the two particles in each pair. The values of L are scaled with the capillary length,

Table 2 Parameters for uncharged particles at the boundary between tetradecane and aqueous solution of 50 mM SDS and 50 mM NaCl

Parameter	Pair 1		Pair 2		Pair 3		Pair 4	
Particle no.	$k = 1$	$k = 2$	$k = 1$	$k = 2$	$k = 1$	$k = 2$	$k = 1$	$k = 2$
R_k/mm	0.308	0.300	0.282	0.269	0.275	0.288	0.281	0.301
$r_{c,k}$/mm	0.230	0.232	0.208	0.189	0.256	0.259	0.261	0.270
θ_k/deg	148	144	146	148	122	128	123	129
$V_{n,k}$/mm^3	0.113	0.103	0.0873	0.0769	0.0664	0.0808	0.0711	0.0925
$V_{w,k}$/mm^3	0.00915	0.00998	0.00663	0.00460	0.0208	0.0193	0.0218	0.0217
$A_{n,k}$/mm^2	0.992	0.924	0.837	0.778	0.649	0.749	0.680	0.821
$A_{w,k}$/mm^2	0.200	0.267	0.162	0.131	0.302	0.293	0.312	0.318
η_k/mPa s	2.061	2.038	2.068	2.094	1.846	1.898	1.850	1.901
$F_{g,k}$/μN	2.156	1.988	1.661	1.449	1.496	1.773	1.595	1.970
$F_{m,k}$/μN	0.051	0.047	0.033	0.025	0.042	0.049	0.046	0.060
$h_{g,k}$/mm	0.132	0.121	0.106	0.096	0.087	0.100	0.092	0.119
$\psi_{g,k}$/deg	15.9	14.5	13.5	12.9	9.8	11.2	10.3	12.3
$\psi_{exp,k}$/deg	16	15	14	13	11	12	11	13

q^{-1}, see Table 1. The dependences in Fig. 7, which are strongly nonlinear, indicate that the motion of the two particles accelerates when the distance between them diminishes.

The points in Fig. 8 represent the same experimental points as in Fig. 7, but now we have plotted $\Theta(L)$ *vs.* t (instead of L *vs.* t), where $\Theta(L) \equiv \Theta_{exp}(t)$ is calculated using eqn (31). The solid lines represent fits of the respective $\Theta(L)$-*vs.*-t dependences using linear regressions. The slopes of the regression lines, denoted by τ_{fit}, are shown in Table 3.

In addition, by means of eqn (30), (32) and (33), using parameter values from Table 2, we have calculated the respective theoretical dependences, $\Theta(t) \equiv \Theta_{theor}(t)$, which are shown by straight dashed lines in Fig. 8. The slopes of the latter lines, which have been calculated from eqn (32), are denoted by τ_{theor}, and listed in Table 3.

First of all, one sees that the strongly nonlinear experimental dependencies $L(t)$ in Fig. 7 are transformed into straight lines when the same data are plotted as $\Theta_{exp}(L)$ *vs.* t in Fig. 8. The theoretical dependences $\Theta_{theor}(t)$ (the dashed lines in Fig. 8) are close to the respective experimental curves, which is seen also from the comparison of τ_{fit} and τ_{theor} in Table 3.

The difference between τ_{fit} and τ_{theor} for some pairs of particles is probably due to the increased hydrodynamic resistance caused by the meniscus formed around each separate particle.[41] Note that the additional friction due to the motion of this meniscus has not been taken into account when

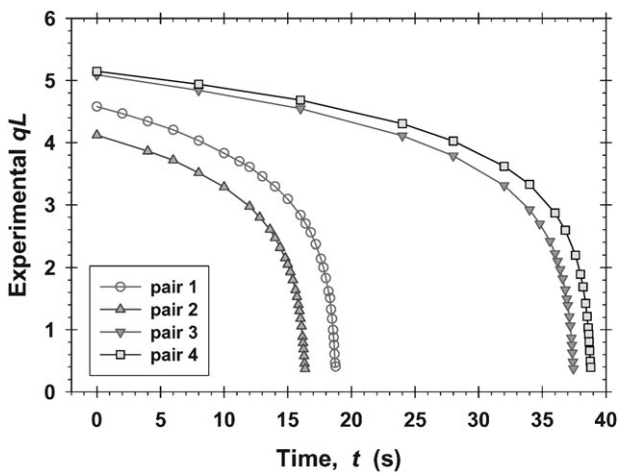

Fig. 7 Experimental interparticle center-to-center distance, L, *vs.* time, t: data for four different pairs of uncharged silanized glass spheres at the interface between tetradecane and aqueous solution of 50 mM SDS + 50 mM NaCl. L is scaled with the capillary length, q^{-1}, see Table 1. The lines are guides to the eye.

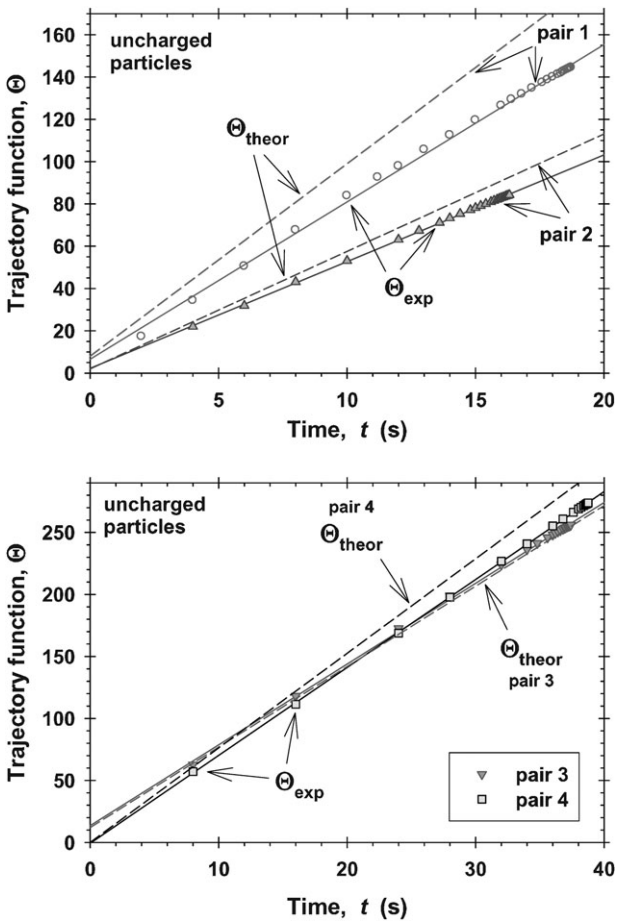

Fig. 8 Plots of the trajectory function, Θ, *vs.* time, t. The symbols denote values $\Theta = \Theta_{exp}$ calculated using eqn (8) and (31) for the experimental points in Fig. 7. The solid lines are fitted by linear regression. The dashed lines represent the theoretical dependence, $\Theta_{theor}(t)$, predicted by eqn (30), along with eqn (32) and (33). (a) Pairs 1 and 2. (b) Pairs 3 and 4.

Table 3 Comparison of the slope, τ_{fit}, determined from the fits of the points in Fig. 8 with the theoretical slope, τ_{theor}, calculated from eqn (32)

Pair no.	τ_{fit}/s^{-1}	τ_{theor}/s^{-1}	$\bar{h}_g$/mm
1	7.55	9.10	0.126
2	5.11	5.55	0.101
3	6.70	6.49	0.094
4	7.08	7.62	0.105

calculating τ_{theor}. Indeed, this additional friction would increase the hydrodynamic resistance β_m, and would decrease the calculated τ_{theor}, see eqn (32). In other words, the deviations of τ_{theor} from τ_{fit} in Table 3 are in the right direction.

To verify the hypothesis that the deviations of τ_{theor} from τ_{fit} are related to the additional hydrodynamic resistance due to the menisci around the particles, in Table 3 we have listed the values of the average depth of these menisci, $\bar{h}_g = (h_{g,1} + h_{g,2})/2$, where $h_{g,1}$ and $h_{g,2}$ are given in Table 2. One sees that the largest deviation of τ_{theor} from τ_{fit} is observed for pair 1, for which $\bar{h}_g$ is the greatest. Moreover, τ_{theor} practically coincides with τ_{fit} for pair 3, for which $\bar{h}_g$ is the smallest.

In conclusion, the linearization of the particle trajectories in Fig. 8, and the close values of τ_{theor} and τ_{fit} in Table 3 indicate that the theoretical approach in Section 3 adequately describes the hydrodynamic interaction between the two particles, despite its approximate character. In general, for uncharged particles we have $\Theta_{theor} \geq \Theta_{exp}$. In particular, the relation $\Theta_{theor} > \Theta_{exp}$ is observed when deeper menisci are formed around the separate particles; the smaller Θ_{exp} could be explained with the additional hydrodynamic resistance due to these menisci.

4.2 Charged particles at tetradecane–pure water interface

Table 4 shows data for the particle pairs No. 5, 6, 7 and 8. The values of R_k, $r_{c,k}$, θ_k and $\psi_{exp,k}$ are experimental (measured from the side-view video frames), whereas the values of the remaining parameters in this table are calculated as explained in Section 3.4. The values of the contact angle, θ_k, varying between 80 and 97°, are smaller than those in Table 2. The interfacial tension, γ, of the tetradecane–pure water boundary is about 10 times greater than that of the solution containing 50 mM SDS, see Table 1. For this reason, the calculated meniscus depth, $h_{g,k}$ in Table 4, is about 10 times smaller than the respective values in Table 2.

The comparison of the last two rows of Table 4 shows that the calculated gravitational meniscus-slope angle, $\psi_{g,k}$, is several times smaller than the experimental meniscus-slope angle, $\psi_{exp,k}$. This fact can be explained by the action of electrodipping force; see also ref. 21.

Fig. 9 shows the experimental time-dependences, $L = L(t)$, of the center-to-center distance between the two particles in each pair. The values of L are scaled with the capillary length, q^{-1}; see Table 1. The slopes of the curves in Fig. 9 increase with the time, t, which indicates acceleration of the particles as they approach each other.

To compare the motion of charged and uncharged particles, in Fig. 10 we have plotted the data for the charged particles in the same way as for the uncharged particles in Fig. 8. One sees that for uncharged particles $\Theta_{theor} \geq \Theta_{exp}$ (Fig. 8), whereas for the charged particles we observe exactly the opposite situation, *viz.* $\Theta_{theor} < \Theta_{exp}$ (Fig. 10). We recall that Θ_{theor} is calculated by assuming that the gravity-induced capillary attraction, alone, is the driving force of the process. The greater values of Θ_{exp} mean that the motion of the charged particles is accelerated in comparison with the hypothetical case described by Θ_{theor}. In other words, the difference between of Θ_{exp} and Θ_{theor} in Fig. 10 indicates that an additional attractive force is acting in the case of two electrically charged particles.

If the additional viscous friction due to the dimples (menisci) formed around the particles were taken into account, it would only decrease the value of Θ_{theor}, thus strengthening the inequality $\Theta_{exp} > \Theta_{theor}$. In other words, the effect of the additional attractive force, which appears as a difference between Θ_{exp} and Θ_{theor} in Fig. 10, is even greater.

It should be also noted that the Θ_{exp}-*vs.*-t curves in Fig. 10 deviate from the simple linear dependence that is observed for uncharged particles in Fig. 8. This deviation could be explained by the fact that only the gravity-induced capillary attraction is accounted for in eqn (31), through the term $K_1(qL)$ in the denominator.

4.3 Charged particles at the interface between tetradecane and water solution of 0.1 mM SDS

The addition of 0.1 mM SDS to the aqueous phase gives rise to a considerable electric-potential difference between the

Table 4 Parameters for electrically charged particles at the boundary between tetradecane and pure water

Parameter / Particle no.	Pair 5		Pair 6		Pair 7		Pair 8	
	$k = 1$	$k = 2$	$k = 1$	$k = 2$	$k = 1$	$k = 2$	$k = 1$	$k = 2$
R_k/mm	0.308	0.259	0.318	0.266	0.296	0.292	0.289	0.249
$r_{c,k}$/mm	0.294	0.237	0.317	0.265	0.294	0.291	0.286	0.247
θ_k/deg	82.6	79.6	90.8	89.8	89.4	95.5	87.7	97.0
$V_{n,k}/mm^3$	0.0346	0.0156	0.0594	0.0343	0.0449	0.0457	0.0397	0.0262
$V_{w,k}/mm^3$	0.0877	0.0572	0.0753	0.0445	0.0637	0.0586	0.0614	0.0384
$A_{n,k}/mm^2$	0.418	0.251	0.585	0.406	0.487	0.491	0.449	0.340
$A_{w,k}/mm^2$	0.774	0.591	0.686	0.483	0.614	0.580	0.600	0.439
η_k/mPa s	1.372	1.297	1.528	1.523	1.502	1.526	1.482	1.495
$F_{g,k}/\mu N$	2.024	1.192	2.277	1.332	1.830	1.762	1.698	1.088
$F_{m,k}/\mu N$	0.011	0.005	0.015	0.006	0.010	0.010	0.009	0.005
$h_{g,k}$/mm	0.018	0.011	0.020	0.012	0.016	0.016	0.015	0.010
$\psi_{g,k}$/deg	1.20	0.88	1.25	0.87	1.08	1.05	1.03	0.77
$\psi_{exp,k}$/deg	9.9	13.4	5.3	8.4	6.1	10.2	6.0	14.3

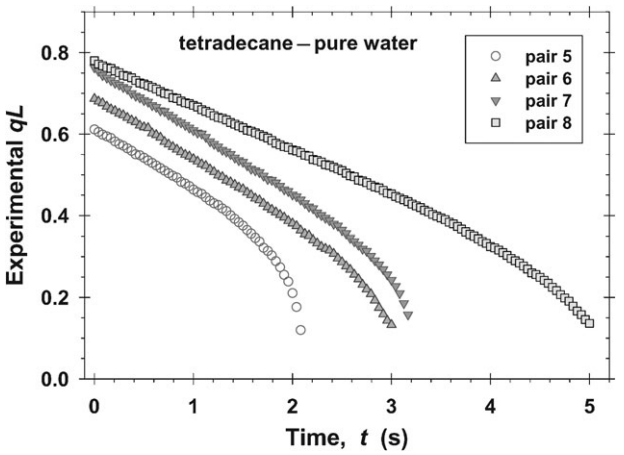

Fig. 9 Experimental interparticle center-to-center distance, L, *vs.* time, t: Data for four different pairs of charged silanized glass spheres at the tetradecane–pure water interface. L is scaled with the capillary length, q^{-1}, see Table 1.

oil–water interface and the bulk of the water phase. This is due to the adsorption of surfactant anions and development of an electric double layer in the aqueous phase near the phase boundary. To estimate these effects, we fitted data for the interfacial tension of aqueous SDS solutions against hexadecane[49] using the van der Waals model.[50,51] At concentration 0.1 mM SDS, the calculated surface potential is −190 mV, the SDS adsorption at the oil–water interface is 6% of the maximum possible, and the surface (Gibbs) elasticity is $E_G = 0.74$ mN m^{-1}. In other words, the presence of 0.1 mM SDS in the water phase gives rise to a relatively high surface electric potential, at a low degree of surface coverage and at a low surface elasticity. Under these conditions, we cannot expect any significant enhancement of the interfacial rheology. Our aim is to see whether the increased surface electric potential produces some effect on the motion of pairs of particles.

Table 5 shows data for the particle pairs No. 9, 10, 11 and 12. As before, the values of R_k, $r_{c,k}$, θ_k and $\psi_{exp,k}$ are experimental (measured from the side-view video frames), whereas the values of the remaining parameters in this table are calculated as explained in Section 3.4. The values of the contact angle, θ_k, varying between 78 and 96°, are smaller than those in Table 2 (uncharged particles), but close to those in Table 4 (charged particles at the tetradecane–water interface). The values of the calculated meniscus depth, $h_{g,k}$, are close to those in Table 4, but much smaller than those in Table 2.

The comparison of the last two rows of Table 5 shows that the calculated gravitational meniscus-slope angle, $\psi_{g,k}$, is several times smaller than the experimental meniscus-slope angle, $\psi_{exp,k}$. By magnitude, the results are very similar to those in Table 4, and can be attributed to the action of electrodipping force due to electric charges located at the particle–oil interface.

Fig. 11 shows the experimental time-dependences, $L = L(t)$, of the center-to-center distance between the two particles in each pair. The curves in Fig. 11 are similar to those in Fig. 9. Their slope increases with the time, t, which indicates acceleration of the particles as they approach each other.

In Fig. 12, we have plotted the data from Fig. 11 as Θ *vs.* t. The results are very similar to those in Fig. 10: for all pairs of

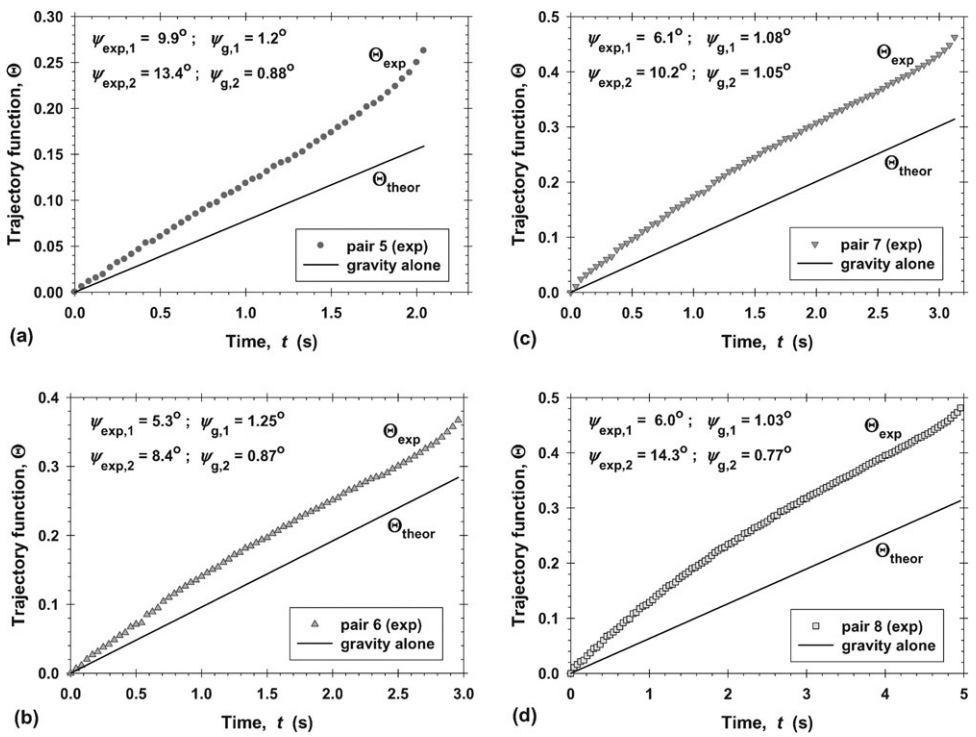

Fig. 10 Plots of the trajectory function, Θ, *vs.* time, t. The symbols denote values $\Theta = \Theta_{exp}$ calculated using eqn (8) and (31) for the experimental points in Fig. 9. The solid lines represent the theoretical dependence, $\Theta = \Theta_{theor}(t)$, predicted by eqn (30), along with eqn (32) and (33). (a) Pair 5; (b) Pair 6; (c) Pair 7, and (d) Pair 8.

Table 5 Parameters for uncharged particles at the boundary between tetradecane and aqueous solution of 0.1 mM SDS without added NaCl

Parameter	Pair 9		Pair 10		Pair 11		Pair 12	
Particle no.	$k = 1$	$k = 2$	$k = 1$	$k = 2$	$k = 1$	$k = 2$	$k = 1$	$k = 2$
R_k/mm	0.267	0.247	0.274	0.230	0.309	0.248	0.275	0.269
$r_{c,k}$/mm	0.266	0.245	0.273	0.229	0.295	0.247	0.272	0.267
θ_k/deg	92.8	90.0	89.3	95.1	78.3	95.1	89.6	93.4
$V_{n,k}$/mm^3	0.0347	0.0256	0.0376	0.0219	0.0350	0.0277	0.0340	0.0334
$V_{w,k}$/mm^3	0.0450	0.0375	0.0486	0.0290	0.0886	0.0362	0.0531	0.0482
$A_{n,k}$/mm^2	0.409	0.335	0.431	0.301	0.421	0. 352	0.405	0.399
$A_{w,k}$/mm^2	0.487	0.432	0.512	0.363	0.778	0. 421	0.545	0.510
η_k/mPa s	1.523	1.494	1.524	1.518	1.372	1.521	1.480	1.498
$F_{g,k}$/μN	1.347	1.062	1.456	0.860	2.044	1.079	1.462	1.372
$F_{m,k}$/μN	0.007	0.005	0.008	0.004	0.013	0.005	0.008	0.008
$h_{g,k}$/mm	0.014	0.012	0.015	0.010	0.021	0.012	0.015	0.015
$\psi_{g,k}$/deg	1.05	0.90	1.10	0.78	1.43	0.91	1.11	1.06
$\psi_{exp,k}$/deg	7.8	7.3	4.2	10.4	5.6	10.2	8.1	10.4

particles, we have $\Theta_{exp} > \Theta_{theor}$. In other words, the motion of the charged particles is accelerated in comparison with the hypothetical case, in which the gravity-induced capillary attraction, alone, is the driving force of the process. Thus, the data in Fig. 12 confirms that an additional attractive force is acting in the case of two like-charged particles. The similarity between the results in Fig. 10 and 12 indicates that the charging of the oil–water interface due to the adsorption of SDS anions from the aqueous phase does not produce any significant effect on the interaction between the two particles.

4.4 Discussion

As established in Sections 4.2 and 4.3, the motion of the charged particles against each other is faster than expected on the basis of the gravity-induced capillary attraction alone (see the results for pairs 5–12 in Fig. 10 and 12). The next question is whether we could identify the acting additional attraction with the electrocapillary force, F_{EC}; see Fig. 1.

First of all, the deformation of the oil–water interface around the investigated charged particles is due to the interplay of gravitational and electric forces; see ref. 25 for details. In particular, because $\psi_{exp,k} >> \psi_{g,k}$, the electric deformation

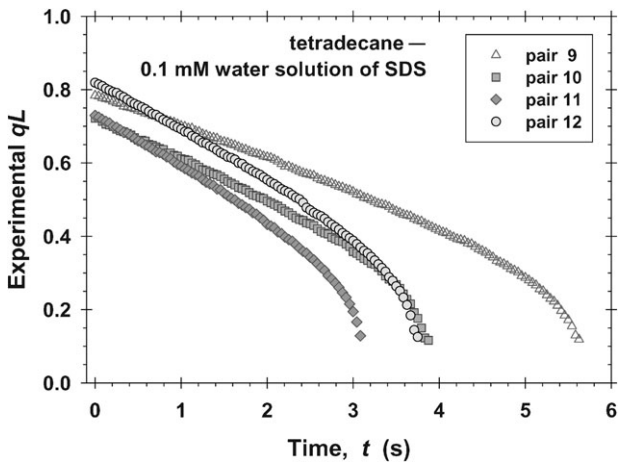

Fig. 11 Experimental interparticle center-to-center distance, L, *vs.* time, t: Data for four different pairs of charged silanized glass spheres at the interface between tetradecane and aqueous solution of 0.1 mM SDS. L is scaled with the capillary length, q^{-1}, see Table 1.

is predominant near the particle. On the other hand, the electric deformation decays much faster than the gravitational one.[25] The latter dominates the interfacial deformation, and the interparticle attraction, at the longer distances.

In principle, it is possible for the interference of the gravitational and electric interfacial deformations, produced by the two particles, to engender a hybrid, gravity-electric capillary force, F_{GE}. This hypothesis is supported by the fact that the deviation of Θ_{exp} from Θ_{theor} is significant at relatively long interparticle separations (see Fig. 9–12), at which the contribution of the purely electric deformations of the oil–water interface is expected to be negligible in comparison with the gravitational deformations; see ref. 25. Qualitatively, F_{GE} could be related to the sliding of one of the two particles over the gravitation-induced meniscus of the other particle under the action of a non-zero tangential projection of the total electric force exerted on the first particle.

A future theoretical analysis could lead to the derivation of an expression for $F_{GE}(L)$. The latter should be taken into account in the right-hand side of eqn (6), and then Θ_{exp} and Θ_{theor} should be recalculated. If we get $\Theta_{exp} \neq \Theta_{theor}$ again, the difference can be attributed to the force difference $F_{EC} - F_{ER}$ (Fig. 1). Finally, F_{EC} could be determined if F_{ER} is calculated, *e.g.* by using the theoretical approach developed in ref. 26.

Oettel *et al.*[28] suggested the idea that the capillary attraction between like charged particles could be due to the existence of an external electric field that gives rise to a force acting on the particles in direction normal to the oil–water interface. In our experiments (here, and in ref. 21 and 25), we have not applied any external electric fields. The quantitative analysis of our data for *single* particles shows that the normal force acting on the particle, $F_{ED} = 2\pi r_c \gamma \sin\psi$, determined from the measured angle ψ, as well as the experimental profile of the liquid meniscus around the particle, $z = \zeta(r)$, can be explained in a self-consistent manner if electric charges of density σ_{pn} are present at the particle–oil interface.[21,25] Fitting the data, we obtained σ_{pn} in the range 20–70 μC m^{-2}, which correspond to 8000–2300 nm^2 per one elementary charge. A value of the same order, $\sigma_{pn} \approx 80$ μC m^{-2}, was reported by other authors[9] for the boundary silanized silica–hydrocarbon. These values of the surface charge density are relatively low, but they are sufficient to explain the observed effects: the magnitudes of

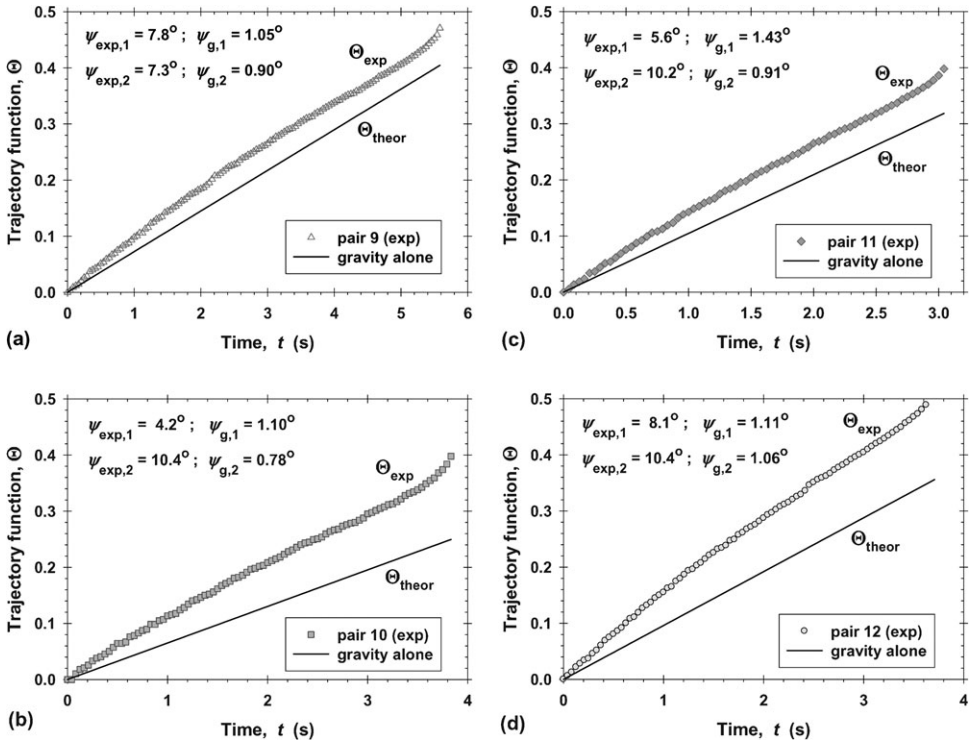

Fig. 12 Plots of the trajectory function, Θ, *vs*. time, *t*. The symbols denote values $\Theta = \Theta_{exp}$ calculated using eqn (8) and (31) for the experimental points in Fig. 11. The solid lines represent the theoretical dependence, $\Theta = \Theta_{theor}(t)$, predicted by eqn (30), along with eqn (32) and (33). (a) Pair 9; (b) pair 10; (c) pair 11, and (d) pair 12.

F_{ED} and $\zeta(r)$,[21,25] as well as the formation of two-dimensional arrays of long interparticle separations under the action of F_{ER}.[6,7,9–11,26] In other words, the accumulated experimental data could be quantitatively interpreted without invoking the hypothesis of the action of an additional external electric field: the field created by the charged particles is strong enough to engender the observed phenomena.

5. Summary and conclusions

In the present study, we investigate experimentally and theoretically the motion of spherical glass particles of radii 240–310 μm attached to the tetradecane–water interface. Pairs of particles, which are moving toward each other under the action of lateral capillary force, are observed by optical microscopy. The purpose of these experiments is to check whether the particle electric charges influence the particle motion, and whether an electric-field-induced capillary attraction could be detected. The particles have been hydrophobized by using two different procedures. The first of them yields particles of contact angle about 90°, which bear electric charges at the oil–water interface. The second procedure produces uncharged particles of contact angles about 140° (Section 2.1). One can establish whether a given particle is charged or uncharged by measuring the meniscus-slope angle, ψ, at the particle contact line. For a charged particle, the magnitude of this angle is increased by the electrodipping force, whereas for uncharged particles such effect is missing (see Tables 2, 4, and 5).

The particle motion is affected by the viscous friction, including the Stokes force acting on a separate particle and the hydrodynamic interaction between the two particles. To quantify these effects, we developed a semiempirical quantitative approach based on the Stimson–Jeffrey formula (Section 3.2). Further, we defined an appropriate trajectory function, $\Theta(t)$, which should increase linearly with time if the particle motion is driven solely by the gravity-induced capillary force. Then, a procedure of data processing is formulated (Section 3.4).

Control experiments with uncharged particles have been carried out to check the procedure for data processing. For these data, the trajectory function is really a straight line, and its experimental and theoretical values practically coincide, $\Theta_{exp} \approx \Theta_{theor}$. For some bigger particles we found $\Theta_{exp} < \Theta_{theor}$, which could be explained by the additional hydrodynamic resistance due to the greater depth of the meniscus formed around such particles (this effect is not taken into account in Θ_{theor}); see Fig. 8 and Section 4.1.

The experimental data for the motion of electrically charged particles were processed exactly in the same way as the results for uncharged particles. A considerable difference between the motion of the two types of particles was found: for the charged particles we have systematically $\Theta_{exp} > \Theta_{theor}$ (Fig. 10 and 12). This means that the motion of the charged particles is accelerated in comparison with the hypothetical case, in which the particle motion is due to the gravity-induced capillary attraction alone. Thus, the results indicate that an additional attractive force is acting in the case of two electrically charged particles (Sections 4.2 and 4.3).

In principle, it is possible for the interference of the gravitational and electric interfacial deformations, produced by the two particles, to engender a hybrid, gravity-electric capillary force. This hypothesis is supported by the fact that the deviation of Θ_{exp} from Θ_{theor} is significant at relatively long interparticle separations, at which the contribution of the purely electric deformations of the oil–water interface is negligible in comparison with the gravitational deformations (Section 4.4). The detailed theoretical explanation of the observed effects is a matter of a future development. The results reported here give an unequivocal evidence for the existence of an additional attraction between two like-charged particles at an oil–water interface. This attraction exceeds the direct electrostatic repulsion between the two particles (across the oil phase) and leads to a noticeable acceleration of their motion.

Acknowledgements

We gratefully acknowledge the consultancy help of Prof. Nikolai Denkov for a part of the experiments. Partial support of COST Action D43 is acknowledged.

References

1 B. P. Binks, Particles as surfactants—similarities and differences, *Curr. Opin. Colloid Interface Sci.*, 2002, **7**, 21–41.
2 R. Aveyard, B. P. Binks and J. H. Clint, Emulsions stabilised solely by colloidal particles, *Adv. Colloid Interface Sci.*, 2003, **100–102**, 503–546.
3 M. F. Hsu, M. G. Nikolaides, A. D. Dinsmore, A. R. Bausch, V. D. Gordon, X. Chen, J. W. Hutchinson, D. A. Weitz and M. Marquez, Self-assembled shells composed of colloidal particles: Fabrication and characterization, *Langmuir*, 2005, **21**, 2963–2970.
4 *Colloidal Particles at Liquid Interfaces*, ed. B. P. Binks and T. S. Horozov, Cambridge University Press, Cambridge, 2006.
5 G. G. Fuller, E. J. Stancik and S. Melle, Particle-laden interfaces: rheology, coalescence, adhesion and buckling, in *Colloidal Particles at Liquid Interfaces*, ed. B. P. Binks and T. S. Horozov, Cambridge University Press, Cambridge, 2006, pp. 169–185.
6 R. Aveyard, J. H. Clint, D. Nees and V. N. Paunov, Compression and structure of monolayers of charged latex particles at air/water and octane/water interfaces, *Langmuir*, 2000, **16**, 1969–1979.
7 R. Aveyard, B. P. Binks, J. H. Clint, P. D. I. Fletcher, T. S. Horozov, B. Neumann, V. N. Paunov, J. Annesley, S. W. Botchway, D. Nees, A. W. Parker, A. D. Ward and A. Burgess, Measurement of long-range repulsive forces between charged particles at an oil–water interface, *Phys. Rev. Lett.*, 2002, **88**, 246102.
8 M. G. Nikolaides, A. R. Bausch, M. F. Hsu, A. D. Dinsmore, M. P. Brenner, C. Gay and D. A. Weitz, Electric-field-induced capillary attraction between like-charged particles at liquid interfaces, *Nature*, 2002, **420**, 299–301.
9 T. S. Horozov, R. Aveyard, J. H. Clint and B. P. Binks, Order-disorder transition in monolayers of modified monodisperse silica particles at the octane–water interface, *Langmuir*, 2003, **19**, 2822–2829.
10 T. S. Horozov, R. Aveyard, B. P. Binks and J. H. Clint, Structure and stability of silica particle monolayers at horizontal and vertical octane–water interfaces, *Langmuir*, 2005, **21**, 7407–7412.
11 T. S. Horozov and B. P. Binks, Particle behavior at horizontal and vertical fluid interfaces, *Colloids Surf., A*, 2005, **267**, 64–73.
12 M. E. Labib and R. Williams, The effect of moisture on the charge at the interface between solids and organic liquids, *J. Colloid Interface Sci.*, 1987, **115**, 330–338.
13 A. P. Philipse and A. Vrij, Preparation and properties of non-aqueous model dispersions of chemically modified, charged silica spheres, *J. Colloid Interface Sci.*, 1989, **128**, 121–136.
14 D. Langevin, Electric-field-induced capillary attraction between like-charged particles at liquid interfaces, *ChemPhysChem*, 2003, **4**, 1057–1058.
15 D. Y. C. Chan, J. D. Henry and R. L. White, The interaction of colloidal particles collected at fluid interfaces, *J. Colloid Interface Sci.*, 1981, **79**, 410–418.
16 V. N. Paunov, P. A. Kralchevsky, N. D. Denkov and K. Nagayama, Lateral capillary forces between floating submillimeter particles, *J. Colloid Interface Sci.*, 1993, **157**, 100–112.
17 P. A. Kralchevsky and K. Nagayama, Capillary forces between colloidal particles, *Langmuir*, 1994, **10**, 23–36.
18 P. A. Kralchevsky and K. Nagayama, Capillary interactions between particles bound to interfaces, liquid films and biomembranes, *Adv. Colloid Interface Sci.*, 2000, **85**, 145–192.
19 P. A. Kralchevsky and K. Nagayama, *Particles at fluid interfaces and membranes*, Elsevier, Amsterdam, 2001.
20 N. D. Vassileva, D. van den Ende, F. Mugele and J. Mellema, Capillary forces between spherical particles floating at a liquid–liquid interface, *Langmuir*, 2005, **21**, 11190–11200.
21 K. D. Danov, P. A. Kralchevsky and M. P. Boneva, Electrodipping force acting on solid particles at a fluid interface, *Langmuir*, 2004, **20**, 6139–6151.
22 L. E. Helseth, R. M. Muruganathan, Y. Zhang and T. M. Fischer, Colloidal rings in a liquid mixture, *Langmuir*, 2005, **21**, 7271–7275.
23 K. D. Danov, P. A. Kralchevsky, K. P. Ananthapadmanabhan and A. Lips, Particle–interface interaction across a nonpolar medium in relation to the production of particle-stabilized emulsions, *Langmuir*, 2006, **22**, 106–115.
24 M. E. Leunissen, A. von Blaaderen, A. D. Hollingsworth, M. T. Sullivan and P. M. Chaikin, Electrostatics at the oil–water interface, stability, and order in emulsions and colloids, *Proc. Natl. Acad. Sci. U. S. A.*, 2007, **104**, 2585–2590.
25 K. D. Danov, P. A. Kralchevsky and M. P. Boneva, Shape of the capillary meniscus around an electrically charged particle at a fluid interface: comparison of theory and experiment, *Langmuir*, 2006, **22**, 2653–2667.
26 K. D. Danov and P. A. Kralchevsky, Electric forces induced by a charged colloid particle attached to the water–nonpolar fluid interface, *J. Colloid Interface Sci.*, 2006, **298**, 213–231.
27 L. Foret and A. Würger, Electric-field induced capillary interaction of charged particles at a polar interface, *Phys. Rev. Lett.*, 2004, **92**, 058302.
28 M. Oettel, A. Domínguez and S. Dietrich, Effective capillary interaction of spherical particles at fluid interfaces, *Phys. Rev. E*, 2005, **71**, 051401.
29 M. Oettel, A. Domínguez and S. Dietrich, Comment on electrodipping force acting on solid particles at a fluid interface, *Langmuir*, 2006, **22**, 846–847.
30 K. D. Danov and P. A. Kralchevsky, Reply to comment on electrodipping force acting on solid particles at a fluid interface, *Langmuir*, 2006, **22**, 848–849.
31 M. Oettel, A. Domínguez and S. Dietrich, Attractions between charged colloids at water interfaces, *J. Phys.: Condens. Matter*, 2005, **17**, L337–L342.
32 A. Würger and L. Foret, Capillary attraction of colloidal particles at an aqueous interface, *J. Phys. Chem. B*, 2005, **109**, 16435–16438.
33 A. Würger, Capillary attraction of charged particles at a curved liquid interface, *Europhys. Lett.*, 2006, **75**, 978–984.
34 O. Gómez-Guzmán and J. Ruiz-Garcia, Attractive interactions between like-charged colloidal particles at the air/water interface, *J. Colloid Interface Sci.*, 2005, **291**, 1–6.
35 W. Chen, S. Tan, T.-K. Ng, W. T. Ford and P. Tong, Long-ranged attraction between charged polystyrene spheres at aqueous interfaces, *Phys. Rev. Lett.*, 2005, **95**, 218301.
36 W. Chen, S. Tan, Z. Huang, T.-K. Ng, W. T. Ford and P. Tong, Measured long-ranged attractive interaction between charged polystyrene latex spheres at a water–air interface, *Phys. Rev. E*, 2006, **74**, 021406.
37 T. Ngai, H. Auweter and S. H. Behrens, Environmental responsiveness of microgel particles and particle-stabilized emulsions, *Macromolecules*, 2006, **39**, 8171–8177.

38 K. D. Danov, B. Pouligny and P. A. Kralchevsky, Capillary forces between colloidal particles confined in a liquid film: the finite-meniscus problem, *Langmuir*, 2001, **17**, 6599–6609.
39 J. T. Petkov, K. D. Danov, N. D. Denkov, R. Aust and F. Durst, Precise method for measuring the shear surface viscosity of surfactant monolayers, *Langmuir*, 1996, **12**, 2650–2653.
40 K. D. Danov, R. Aust, F. Durst and U. Lange, Influence of the surface viscosity on the hydrodynamic resistance and surface diffusivity of a large Brownian particle, *J. Colloid Interface Sci.*, 1995, **175**, 36–45.
41 J. T. Petkov, N. D. Denkov, K. D. Danov, O. D. Velev, R. Aust and F. Durst, Measurement of the drag coefficient of spherical particles attached to fluid interfaces, *J. Colloid Interface Sci.*, 1995, **172**, 147–154.
42 K. D. Danov, R. Dimova and B. Pouligny, Viscous drag of a solid sphere straddling a spherical or flat surface, *Phys. Fluids*, 2000, **12**, 2711–2722.
43 T. M. Fischer, P. Dhar and P. Heinig, The viscous drag of spheres and filaments moving in membranes or monolayers, *J. Fluid Mech.*, 2006, **558**, 451–475.
44 M. Stimson and G. B. Jeffrey, The motion of two spheres in a viscous fluid, *Proc. R. Soc. London, Ser. A*, 1926, **111**, 110–116.
45 G. I. Taylor, private communication acknowledged by W. Hardy and I. Bircumshaw, Bakerian lecture: Boundary lubrication; plane surfaces and the limitations of Amontons' law, *Proc. R. Soc. London, Ser. A*, 1925, **108**, 1–27.
46 I. B. Ivanov, Effect of surface mobility on the dynamic behavior of thin liquid films, *Pure Appl. Chem.*, 1980, **52**, 1241–1262.
47 C. W. Nutt, Froth flotation: The adhesion of solid particles to flat interfaces and bubbles, *Chem. Eng. Sci.*, 1960, **12**, 133–141.
48 I. B. Ivanov, P. A. Kralchevsky and A. D. Nikolov. Film, line tension effects on the attachment of particles to an interface, *J. Colloid Interface Sci.*, 1986, **112**, 97–107.
49 T. D. Gurkov, D. T. Todorova, K. G. Marinova, C. Bilke-Crause, C. Gerber and I. B. Ivanov, Ionic surfactants on fluid interfaces: determination of the adsorption; role of the salt and the type of the hydrophobic phase, *Colloids Surf., A*, 2005, **261**, 29–38.
50 P. A. Kralchevsky, K. D. Danov, G. Broze and A. Mehreteab, Thermodynamics of ionic surfactant adsorption with account for the counterion binding: effect of salts of various valency, *Langmuir*, 1999, **15**, 2351–2365.
51 V. L. Kolev, K. D. Danov, P. A. Kralchevsky, G. Broze and A. Mehreteab, Comparison of the van der Waals and Frumkin adsorption isotherms for sodium dodecyl sulfate at various salt concentrations, *Langmuir*, 2002, **18**, 9106–9109.

